Geophys. J. Int. (2009) **179,** 1279–1291 doi: 10.1111/j.1365-246X.2009.04371.x

GPS-derived coupling estimates for the Central America subduction zone and volcanic arc faults: El Salvador, Honduras and Nicaragua

F. Correa-Mora,[1] C. DeMets,[1] D. Alvarado,[1] H. L. Turner,[2] G. Mattioli,[2] D. Hernandez,[3] C. Pullinger,[4] M. Rodriguez[5] and C. Tenorio[5]

[1] *Geology and Geophysics, University of Wisconsin-Madison, Madison,* WI 53706*, USA. E-mail: chuck@geology.wisc.edu*
[2] *Department of Geosciences, University of Arkansas, Fayetteville, AR, USA*
[3] *Servicio Nacional de Estudios Territoriales, Ministerio de Medio Ambiente y Recursos Naturales Km.* 5 1/2 *carretera a Santa Tecla, Colonia y Calle Las Mercedes, Plantel ISTA San Salvador, El Salvador*
[4] *LaGeo S.A. de C.V.,* 15 *Av. Sur, Colonia Utila, Santa Tecla, La Libertad, El Salvador*
[5] *School of Physics, Faculty of Sciences, Universidad Nacional Autonoma de Honduras, Tegucigalpa, Honduras*

Accepted 2009 August 24. Received 2009 August 24; in original form 2009 January 4

SUMMARY

We invert GPS velocities from 32 sites in El Salvador, Honduras and Nicaragua to estimate the rate of long-term forearc motion and distributions of interseismic coupling across the Middle America subduction zone offshore from these countries and faults in the Salvadoran and Nicaraguan volcanic arcs. A 3-D finite element model is used to approximate the geometries of the subduction interface and strike-slip faults in the volcanic arc and determine the elastic response to coupling across these faults. The GPS velocities are best fit by a model in which the forearc moves 14–16 mm yr^{-1} and has coupling of 85–100 per cent across faults in the volcanic arc, in agreement with the high level of historic and recent earthquake activity in the volcanic arc. Our velocity inversion indicates that coupling across the potentially seismogenic areas of the subduction interface is remarkably weak, averaging no more than 3 per cent of the plate convergence rate and with only two poorly resolved patches where coupling might be higher along the 550-km-long segment we modelled. Our geodetic evidence for weak subduction coupling disagrees with a seismically derived coupling estimate of 60 $\pm$ 10 per cent from a published analysis of earthquake damage back to 1690, but agrees with three other seismologic studies that infer weak subduction coupling from 20th century earthquakes. Most large historical earthquakes offshore from El Salvador and western Nicaragua may therefore have been intraslab normal faulting events similar to the M_w 7.3 1982 and M_w 7.7 2001 earthquakes offshore from El Salvador. Alternatively, the degree of coupling might vary with time. The evidence for weak coupling indirectly supports a recently published hypothesis that much of the Middle American forearc is escaping to the west or northwest away from the Cocos Ridge collision zone in Costa Rica. Such a hypothesis is particularly attractive for El Salvador, where there is little or no convergence obliquity to drive the observed trench-parallel forearc motion.

Key words: Continental neotectonics; Kinematics of crustal and mantle deformation.

1 INTRODUCTION

Along the Pacific coast of Central America, convergence between the Cocos and Caribbean plates is accommodated by a combination of 70–85 mm yr^{-1} of northeast-directed Cocos Plate subduction (Fig. 1) and ~10–15 mm yr^{-1} of northwestward trench-parallel motion of areas outboard from the volcanic arc (White 1991; DeMets 2001; Dewey *et al.* 2004; Turner *et al.* 2007). Associated with these processes, destructive volcanic arc earthquakes in El Salvador and Nicaragua have occurred every several years over the past century (White 1991; White & Harlow 1993) and every ~70 yr offshore along or close to the Cocos Plate subduction interface (Satake 1994; Bommer *et al.* 2002; Benito *et al.* 2004; White *et al.* 2004). These earthquakes have caused nearly 20 000 fatalities in the past century (White & Harlow 1993), underscoring the importance of better understanding their sources and causes.

Given the historic record, it is important to quantify the rate that elastic strain presently accumulates across the subduction interface and faults in the volcanic arc. Studies of the abundant historic and modern seismicity of the volcanic arc faults (White 1991; White & Harlow 1993) and their surface expressions (e.g. Cowan *et al.* 2002; La Femina *et al.* 2002; Corti *et al.* 2005; Agostini *et al.*

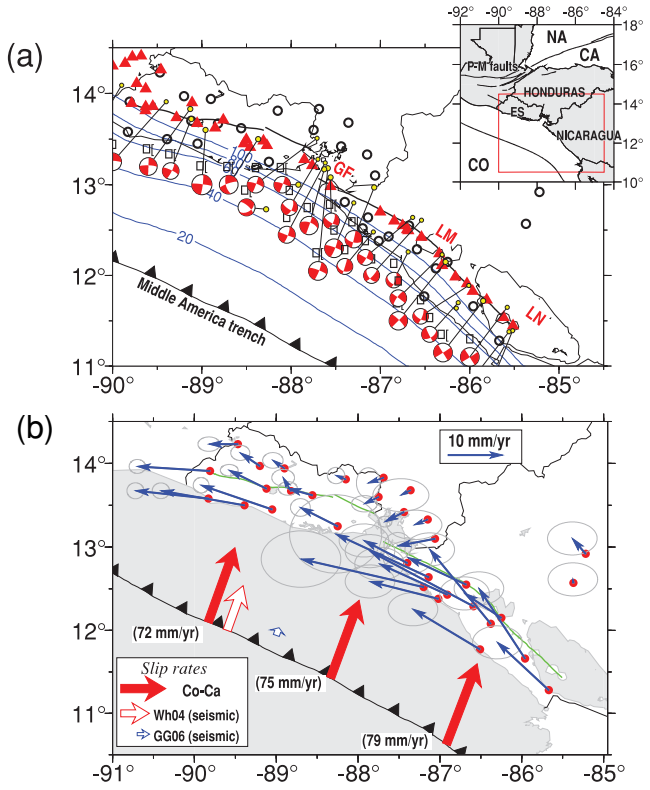

Figure 1. (a) Location map and tectonic setting of the study area in Central America. Black open circles show GPS site locations; red triangles show volcanos; black solid lines show volcanic arc faults. Focal mechanisms are shown for the period of 1963–2001 Feburary (DeMets 2001). Blue contour lines delineate the depth of the subduction interface from Funk *et al.* (2009). Inset shows major tectonic features and plate boundaries. GF,Gulf of Fonseca; LM, Lake Managua; LN, Lake Nicaragua; NA, North America Plate; CA, Caribbean Plate; CO, Cocos Plate and P-M, Polochic-Motagua faults. (b) GPS site velocities relative to Caribbean Plate determined from data described by Turner *et al.* (2007) and Alvarado (2008). Uncertainty ellipses are 2-D, 1σ. Solid red arrows indicate the Cocos–Caribbean Plate direction and rates (in parentheses) predicted by the PVEL plate motion model (DeMets *et al.*, 'Geologically recent plate motions', manus. in review., 2009). Open arrows show seismic slip rates (GG06) from Guzman-Speziale & Gomez-Gonzalez (2006) and a seismic slip rate for western El Salvador (Wh04) converted from historic cumulative seismic slip shown in fig. 7 of White *et al.* (2004). Green solid lines approximate volcanic arc fault locations.

2006; Funk *et al.* 2009) have advanced our understanding of their seismogenic hazards. Complementing such work, Coulomb failure stress modelling has been used to better understand how past and future earthquakes along faults in the volcanic arcs of El Salvador and Nicaragua may be influenced by subduction zone earthquakes (Martinez-Diaz *et al.* 2004) and rheologically weak volcanic zones (Cailleau *et al.* 2007). Nothing however has been published about the degree of interseismic coupling across the faults within either of the two volcanic arcs.

Significantly more has been published about the degree of long-term seismic coupling across the subduction interface offshore from El Salvador and Nicaragua. McNally & Minster (1981) estimate that little or no seismic slip has occurred during the past century along the subduction interface offshore from El Salvador and the western half of Nicaragua, which they attribute to partial decoupling of the subduction interface due to down bending of the subducting plate. Pacheco *et al.* (1993) similarly conclude that coupling has been weak based on their analysis of earthquakes from a similarly long period. From the shorter, but more complete global centroid moment tensor catalogue, Guzman-Speziale & Gomez-Gonzalez (2006) use thrust faulting earthquakes recorded between 1976 and 2003 to derive a seismic coupling estimate of ~10 per cent (open blue arrow in Fig. 1b) for the subduction zone offshore from El Salvador, Guatemala and Nicaragua.

In contrast to the above studies, White *et al.* (2004) estimate a higher degree of seismic coupling from their compilation of regional historical records of earthquake damage dating back to 1526. Based on their approximation of the moment magnitudes of the largest historical earthquakes since 1690, they estimate that the cumulative slip for large offshore earthquakes has equalled 60 ± 10 per cent of the total plate convergence beneath western El Salvador (open red arrow in Fig. 1b).

The discrepancy between the White *et al.* estimate of the degree of seismic coupling and the other seismologic estimates described above has at least two possible explanations. The low rate of subduction-thrust earthquakes over the past century may reflect a possibly long recurrence interval for such events offshore from El Salvador and western Nicaragua. Alternatively, White *et al*. note that their estimate of the cumulative seismic slip may include large intraslab normal faulting events, similar to those that occurred offshore from El Salvador in 1982 (M_w 7.3) and 2001 (M_w 7.7) (Fig. 2c). If so, these earthquakes must be excluded from any calculation of the seismic slip rate along the subduction interface.

Geodetic measurements that were initiated in Central America in the late 1990s offer an independent means of discriminating between the strongly and weakly coupled scenarios outlined above. Full interseismic coupling of the offshore subduction interface would cause stations within a few hundred kilometres of the trench to accrue elastic shortening at rates of 10 mm yr^{-1} or faster towards the plate interior (Fig. 3b) given the plate convergence rate of 70–80 mm yr^{-1} across this part of the Middle America trench. The elastic effects of coupling as low as ~10 per cent could thus be measured easily with GPS given that GPS velocity uncertainties are typically ±1–2 mm yr^{-1} after several years of measurements.

From GPS measurements at coastal sites in Guatemala, just east of our study area, Lyon-Caen *et al.* (2006) instead report that stations move nearly parallel to the trench and infer weak coupling from elastic half-space modelling of their GPS station velocities. Turner *et al.* (2007) and Alvarado (2008) also report that GPS stations inland from the trench in Nicaragua and El Salvador move nearly parallel to the trench (Fig. 1b) and from these infer that coupling across the subduction interface is weak. Similarly, finite element modelling of GPS station velocities from Costa Rica and Nicaragua also indicates that coupling offshore Nicaragua is weak, with the exception of possible stronger coupling at depths above 20 km (LaFemina *et al.* 2009).

Herein, we use GPS velocity fields (Fig. 1b) from El Salvador (Alvarado 2008), Honduras (Rodriguez *et al.* 2009) and Nicaragua (Turner *et al.* 2007) to quantify the rate of trench-parallel motion of the Nicaraguan and Salvadoran forearcs and the degree of interseismic coupling across the Middle America subduction interface offshore from these countries and across faults within the Central American volcanic arc. Elastic deformation that is predicted with a 3-D finite element mesh that approximates the geometry of the subduction interface and volcanic arc faults forms the basis for our GPS velocity inversions. We exploit features of our bounded-variable inverse technique to explore the limits of the model estimates. Our results are relevant to seismic hazard and crustal deformation studies in this region and elsewhere in Central America (Lyon-Caen

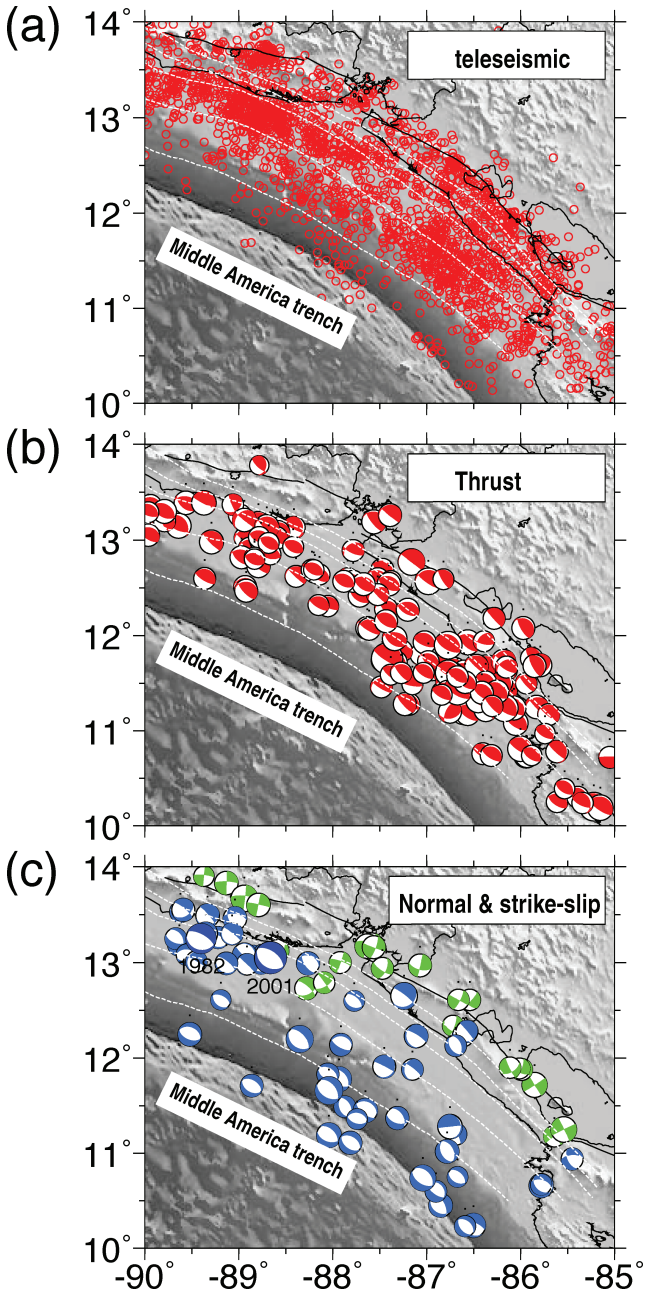

Figure 2. (a) Relocated teleseismic earthquake locations for the period 1964–2006 (Engdahl *et al.* 1998). Dashed white lines show subduction depth contours. (b) Thrust-faulting earthquakes from the global centroid moment tensor catalogue for the period 1976–2008 August. (c) Normal-faulting (blue) and strike-slip (green) earthquakes from the global centroid moment tensor catalogue, 1976–2008 August. The M_w 7.3 1982 June 19 and M_w 7.7 2001 January 13 intraslab normal-faulting earthquakes are labelled in the figure.

et al. 2006; Alvarez-Gomez *et al.* 2008; Rodriguez *et al.* 2009), as well as areas such as the Shumagin Islands of the Alaska-Aleutian subduction zone, where weak subduction coupling and arc-parallel deformation both occur (Fournier & Freymueller 2007).

2 GPS SITE VELOCITIES

The GPS velocities we use come from sites located in Honduras (6), El Salvador (12) and Nicaragua (14) (Fig. 1b and Table 1), and

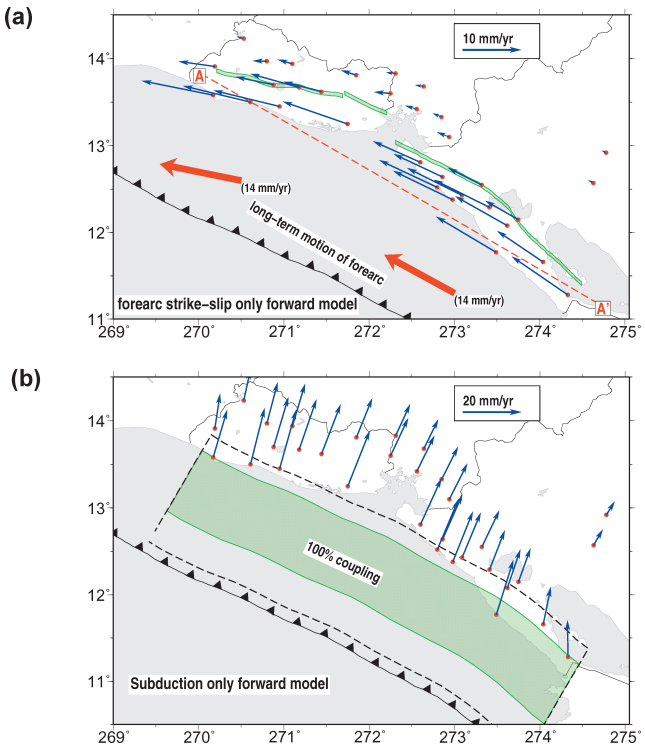

Figure 3. Forward models of the elastic response for fully coupled strike-slip faults in the volcanic arc and a fully coupled subduction interface. Calculations are based on the 3-D mesh shown in Fig. 4. (a) Elastic velocities predicted at GPS station locations for forearc strike-slip faults that are assumed to be fully coupled down to a maximum depth of 20 km, forearc motion of 14 mm yr^{-1}, and zero coupling on the subduction interface. Profile A–A' is used to show inversion results from Fig. 5. (b) Elastic velocities predicted at GPS station locations for a subduction interface that is fully coupled from 20 to 60 km at the full plate convergence rate, in accord with the observed seismicity (Fig. 2b), and no coupling across the volcanic arc faults. Green shaded region shows area of full coupling used to drive the model. Dashed line delineates the entire area of the subduction interface used for our inverse modelling.

are derived from measurements at three continuous stations and 29 campaign sites. Turner *et al.* (2007) and Rodriguez *et al.* (2009) describe in detail the Nicaraguan and Honduran data and the procedures used to analyse the raw GPS data and determine individual station velocities. Detailed information about the Salvadoran GPS velocity field is given by Alvarado (2008) and Alvarado *et al.* ('Forearc motion and deformation between El Salvador and Nicaragua', in preparation 2009). Information about the GPS velocities used herein is summarized briefly below.

All GPS data used for this study were processed using a standard precise point positioning analysis strategy and GIPSY software from the Jet Propulsion Laboratory (Zumberge *et al.* 1997) to determine loosely constrained, no-fiducial daily station coordinates. The daily coordinates at each site were transformed to ITRF2005 (Altamimi *et al.* 2007) and were corrected for common-mode daily and longer-term noise and offsets from nearby earthquakes. Linear regressions of the corrected daily coordinates were used to find station velocities relative to ITRF2005, after which the station velocities were transformed to a common Caribbean Plate reference frame using an angular velocity that specifies the motion of the Caribbean Plate relative to ITRF2005. The angular velocity we used (37.8°N, 98.5°W, 0.262° Myr^{-1}) best fits the motions of 17 GPS stations located in the Caribbean Plate interior (not shown) and agrees closely

Table 1. GPS station velocity information.

Site name	Latitude (°N)	Longitude (°E)	V_n	V_e	Correlation coeff.	V_v
ACAJ (ES)	13.58	−89.83	1.4 ± 1.0	−13.4 ± 1.0	−0.0389	−1.2 ± 1.5
AHUA (ES)	13.91	−89.81	0.8 ± 0.8	−13.3 ± 1.0	−0.0421	−2.5 ± 2.2
CEGD (ES)	13.94	−88.90	1.5 ± 0.9	−2.1 ± 1.2	−0.0280	3.8 ± 2.1
CH15 (ES)	13.62	−88.56	1.3 ± 0.8	−4.5 ± 1.1	−0.0376	3.6 ± 1.9
DERA (ES)	13.67	−88.82	2.5 ± 1.0	−1.4 ± 1.4	−0.0256	2.6 ± 2.4
GUAJ (ES)	14.23	−89.47	0.0 ± 0.9	−5.3 ± 1.3	−0.0267	4.6 ± 1.9
JUCU (ES)	13.25	−88.25	3.4 ± 1.1	−6.8 ± 1.2	−0.0297	10.3 ± 2.5
MNGO (ES)	13.97	−89.20	2.4 ± 0.9	−3.6 ± 1.2	−0.0314	4.3 ± 1.6
OSIC (ES)	13.81	−88.15	0.7 ± 1.0	−1.8 ± 1.1	−0.0313	1.4 ± 1.5
SSAS (ES)	13.45	−89.05	4.5 ± 0.9	−13.0 ± 1.0	−0.0429	8.2 ± 2.4
SSIA (ES)	13.70	−89.12	3.4 ± 0.7	−6.8 ± 1.1	−0.1331	6.4 ± 0.8
SUNZ (ES)	13.50	−89.39	2.7 ± 1.0	−15.3 ± 1.0	−0.0385	8.5 ± 2.4
CARI (HND)	13.83	−87.69	−1.0 ± 1.8	−2.8 ± 1.4	−0.0119	7.8 ± 4.8
LJAS (HND)	13.60	−87.75	−1.2 ± 1.0	−2.6 ± 1.6	−0.0219	1.8 ± 5.3
NDAM (HND)	13.68	−87.36	−0.9 ± 2.0	−1.8 ± 3.4	−0.0048	2.5 ± 5.9
RECA (HND)	13.33	−87.15	−1.0 ± 1.8	−2.4 ± 3.3	−0.0059	0.6 ± 4.8
SGTO (HND)	13.10	−87.06	−1.3 ± 1.6	−6.8 ± 1.7	−0.0136	−1.7 ± 5.6
SLOR (HND)	13.42	−87.44	−1.8 ± 0.7	−3.5 ± 0.8	−0.0506	7.4 ± 10.0
ANA1 (NIC)	12.08	−86.38	13.6 ± 3.2	−11.2 ± 5.1	−0.0027	−11.1 ± 7.7
CHIN (NIC)	12.64	−87.14	7.9 ± 4.7	−17.0 ± 5.6	−0.0016	7.8 ± 9.0
CORI (NIC)	12.52	−87.20	5.1 ± 3.4	−22.5 ± 4.8	−0.0026	3.4 ± 7.6
ELBQ (NIC)	11.28	−85.67	8.8 ± 2.5	−9.4 ± 3.2	−0.0062	1.5 ± 4.8
ELCO (NIC)	12.81	−87.40	4.1 ± 3.5	−7.9 ± 5.0	−0.0023	7.0 ± 7.5
LEON (NIC)	12.43	−86.91	5.6 ± 3.3	−12.4 ± 4.8	−0.0027	−1.5 ± 7.6
MALP (NIC)	12.55	−86.68	5.0 ± 2.7	−10.7 ± 5.5	−0.0028	9.3 ± 6.7
MANA (NIC)	12.15	−86.25	4.5 ± 1.3	−6.7 ± 1.4	−0.0331	4.0 ± 1.9
OCHO (NIC)	11.66	−85.96	12.9 ± 4.4	−8.5 ± 5.6	−0.0019	2.8 ± 8.7
PAZC (NIC)	12.29	−86.59	10.1 ± 3.7	−19.0 ± 5.0	−0.0023	3.8 ± 7.8
POCH (NIC)	11.77	−86.51	7.4 ± 3.5	−12.3 ± 5.0	−0.0027	−0.3 ± 7.6
PONE (NIC)	12.38	−87.02	3.2 ± 4.1	−12.5 ± 5.7	−0.0019	1.4 ± 9.5
PORT (NIC)	12.57	−85.37	0.7 ± 3.9	−0.1 ± 5.9	−0.0016	2.2 ± 8.5
RIOB (NIC)	12.92	−85.22	2.8 ± 3.7	−2.4 ± 7.0	−0.0013	5.0 ± 9.3

Notes: GPS stations are grouped by their country of origin, consisting of El Salvador (ES), Honduras (HND) and Nicaragua (NIC). North (V_n) and east (V_e) components of site velocities are given relative to Caribbean Plate and are in units of millimetres per year. Vertical site motions (V_v) are relative to ITRF2005. Uncertainties are standard errors. The correlation coefficient specifies the dependence between the north and east velocity uncertainties.

with that determined by DeMets *et al.* (2007). Uncertainties in the Caribbean Plate angular velocity are propagated rigorously into the station velocity uncertainties.

The velocities at the stations in El Salvador (Table 1) are determined from annual 1-week or longer occupations between early 2004 and mid-2008 at all but one site and continuous measurements at site SSIA (Alvarado 2008). The Salvadoran station velocities are better determined than for most sites in Honduras and Nicaragua, where the site occupations were typically more irregular and shorter than was the case for the Salvadoran sites. No earthquakes large enough to offset the GPS stations in El Salvador (and Honduras) have occurred since we began measurements at those sites. Consequently, the Salvadoran (and Honduran) GPS velocities record the interseismic velocity field.

Some of the Nicaraguan station measurements began in 1999 (Turner *et al.* 2007), before the M_w 7.7 2001 January 13 intraslab normal faulting earthquake offshore from El Salvador (Bommer *et al.* 2002; Martinez-Diaz *et al.* 2004). Turner *et al.* (2007) use elastic half-space modelling of offsets that were recorded at GPS stations operating during the 2001 January 13 earthquake to estimate the coseismic offsets at all of the Nicaraguan GPS stations and correct their coordinate time-series for these offsets prior to estimating their velocities. The imperfectly known elastic corrections introduce additional, hard-to-quantify uncertainties into the Nicaraguan station velocities (Table 1), possibly accounting for the larger misfits to the Nicaraguan velocities that are described in later section.

3 FINITE ELEMENT MESH AND INVERSE PROCEDURE

3.1 Mesh of western Central America

We model deformation in our study area using finite element modelling software ABAQUS and a 3-D mesh that approximates the geometry of the Middle America subduction zone and volcanic arc faults. Our finite element model (FEM) consists of a denser mesh that is centred on the study area (upper mesh in Fig. 4) and is embedded in a regional mesh whose dimensions are large enough to minimize any edge effects in the study area (lower mesh in Fig. 4). The upper surface of the mesh is constructed from topography and seafloor bathymetry (Smith & Sandwell 1997). The nodes that make up the mesh are spaced by ∼15 km offshore, ∼7 km for regions near the volcanic arc faults, and ∼30 km for regions farther inland. Layers in the mesh allow for vertical variations in its properties, with

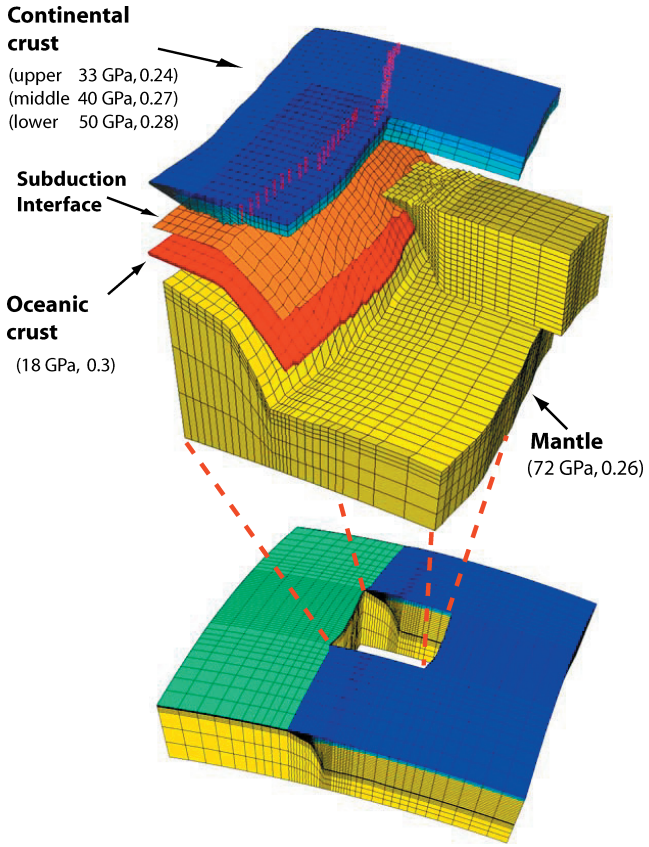

Figure 4. Expanded view of the 3-D finite element mesh used to approximate deformation of the study area. Red dots show nodes that represent the volcanic arc faults and extend to depths of ∼20 km. The upper surface of the mesh is defined by continental topography and seafloor bathymetry from Smith & Sandwell (1997). Numerals in parentheses show shear modulus and Poisson's ratio values assigned to each layer. These values and the thickness for each layer are derived from the seismically based CRUST2 model (Bassin *et al.* 2000). The mesh is built assuming a spherical Earth and is embedded within a regional mesh (bottom panel) with lower and lateral boundaries far from the study area to avoid modelling artefacts.

the assigned elastic properties estimated from the CRUST2 model (Bassin *et al.* 2000). A major discontinuity in the elastic properties occurs at the subduction interface (Fig. 4).

We use slab-depth contours that are based on four depth cross-sections of National Earthquake Information Center hypocentres offshore from El Salvador and Nicaragua (Funk *et al.* 2009) to define the geometry of the subduction interface (orange layer in Fig. 4). The steeply dipping interface agrees with previous work that also defines a steeply dipping slab in this region (Molnar & Sykes 1969; Burbach *et al.* 1984; White & Harlow 1993).

We approximate the geometry of the faults in the volcanic arc using two fault segments in El Salvador and one fault segment in Nicaragua (Figs 1 and 4). Two segments are offset by 40 km across the Gulf of Fonseca, where the volcanic arc in Nicaragua steps ∼40 km inland to the Salvadoran volcanic arc across the Fonseca pull-apart zone (Funk *et al.* 2009; Alvarado 2008). In western and central El Salvador, the fault trace follows well-defined strike-slip faults in the volcanic arc (Corti *et al.* 2005; Agostini *et al.* 2006). The locus of strike-slip faulting in eastern El Salvador is unclear (Alvarado 2008). We therefore use the volcanic arc to approximate the fault location.

In Nicaragua, structural and seismic evidence indicates that northwest movement of the forearc is accommodated by a combination of book-shelf and strike-slip faulting across a ∼25-km-wide zone that mainly follows the volcanic arc (La Femina *et al.* 2002; Funk *et al.* 2009). We do not attempt to incorporate the many possibly active faults into our mesh, but instead approximate the influence of this possibly broad shear zone with a single strike-slip fault that follows the volcanic arc. For this reason, our estimate of coupling in Nicaragua may represent the overall elastic resistance to shear across this zone. The Managua graben, which offsets the Nicaraguan volcanic arc by ∼10 km (Funk *et al.* 2009), is represented by several nodes that define an oblique releasing bend along the volcanic arc (Fig. 3a).

The nodes that represent the volcanic arc faults (shown by red circles in the continental crust of Fig. 4) are located at the surface and depths of ∼8, ∼15 and ∼22 km. Coupling is thus permitted to extend to depths slightly below the maximum depth of crustal seismicity reported by White (1991).

3.2 Mesh boundary conditions and validation

We applied the following constraints while modelling deformation with the mesh: (1) the lateral edges of the mesh for areas located inland from both the subduction interface and translating forearc sliver are pinned; (2) the lateral edges of the oceanic slab are allowed to move; (3) the forearc wedge, which is located between the subduction interface and faults in the volcanic arc, is permitted to translate parallel to those features and (4) nodes at the base of the mesh are permitted to translate horizontally, but not vertically.

We tested our mesh to validate that it predicts the same interseismic elastic velocities as analytically derived solutions for a dipping thrust fault and an infinitely long, vertical strike-slip fault (Okada 1985). For the test, we applied homogeneous elastic properties throughout the mesh to permit a meaningful comparison to the velocities predicted from the analytical elastic half-space solution. In both cases, the interseismic motions predicted from our FEM and the analytical models agree to fractions of a millimetre per year, much smaller than our data and model uncertainties. The good agreement validates the boundary conditions that we apply to the mesh and the approach we adopt for modelling interseismic strike-slip motion.

3.3 Inverse estimation of fault coupling distribution

Herein, we define fault coupling as the absolute ratio of the estimated elastic slip rate deficit at an individual fault node to the full plate convergence rate predicted at that node location. These ratios, which we also refer to as the 'degree of coupling', range from 0 per cent for nodes where plate convergence is accommodated by free slip to 100 per cent for nodes where the elastic slip rate deficit is equal in magnitude, but opposite in sense to the long-term fault slip rate. Considerable debate surrounds the terminology that should be used to describe slip behaviour along a fault or subduction interface during the interseismic phase (Wang & Dixon 2004; Lay & Schwartz 2004). Our modelling provides a kinematic estimate of the elastic slip rate deficit along a fault or subduction interface. Consequently, the term 'coupling' conveys no explicit information about the local frictional state of the fault.

We estimate the degree of coupling at each fault node using the FEM described in the previous section and a bounded-variable inverse procedure summarized below and described in detail by

Correa-Mora *et al.* (2008). Green's functions that constitute the elastic response at each GPS station for a unit back-slip motion at each fault node are generated from the mesh at the nodes that define the subduction interface and the volcanic arc faults. Along with the GPS velocities and their uncertainties, these form the basis for the data inversion. Through forward modelling with the FEM, we constructed the Green's function matrix **G** prior to the data inversion. Calculations of the Green's functions for nodes along the subduction interface are described in detail by Correa-Mora *et al.* (2008).

For the nodes that represent the volcanic arc faults, we calculate the Green's functions in two stages. We first calculate the elastic response at each GPS site to an assumed unit displacement at each volcanic arc fault node in the direction of the long-term forearc motion (the coseismic response). We then subtract this elastic response from an assumed long-term slip rate of the forearc relative to the Caribbean Plate at each GPS site, yielding its interseismic motion. The direction of each forearc node is calculated from the pole that best fits the measured directions of the GPS stations in the Nicaraguan and Salvadoran forearcs relative to the Caribbean Plate (3.2°N, 91.4°W). This pole predicts motion at most sites that is parallel or nearly parallel to the volcanic arc faults. We also experimented with models in which we forced the forearc to translate purely parallel to the trench, but found that such models fit the velocity field more poorly.

We estimate the magnitude of the coupling at each of the m nodes that define the subduction interface and volcanic arc faults by solving the linear system $\mathbf{Gm} = \mathbf{d}$, where $\mathbf{d}$ is a $3n$-element vector that contains the GPS site velocities at n GPS sites, $\mathbf{m}$ is the vector that contains the best estimate of the coupling coefficient at each node that defines the subduction interface and volcanic arc faults, and $\mathbf{G}$ is a $3n$ by m matrix with the Green's functions.

For modelling of the GPS velocity field, we use a bounded-variable least-squares algorithm described by Stark & Parker (1995) to account for all of the constraints, as follows:

$$\begin{bmatrix} \mathbf{WG} \\ \alpha\mathbf{F} \end{bmatrix} \mathbf{m} = \begin{bmatrix} \mathbf{Wd} \\ 0 \end{bmatrix}, \quad (1)$$

where α is the smoothing coefficient, $\mathbf{F}$ is the smoothing matrix, and $\mathbf{W}$ is a square diagonal weighting matrix that contains the reciprocal of the data uncertainties. The smoothing constraints $\alpha\mathbf{F}$ are treated as pseudo-data and are applied downdip and along-strike. Progressively larger values of the smoothing coefficient are associated with increased smoothing. A rigorous procedure for optimizing the smoothing coefficient α is described by Correa-Mora *et al.* (2008) and is applied here.

4 RESULTS: INVERSE MODELLING OF GPS VELOCITY FIELD

Figs 5–7 show the best-fitting inversion results and distributions of coupling along the volcanic arc faults and subduction interface. We identified the best-fitting model by systematically exploring a range of plausible smoothing coefficients and long-term forearc motions from 9 to 19 mm yr^{-1} (Fig. 5d). A smoothing coefficient of $\alpha = 0.7$ optimizes the trade-off between reduced chi-square (the least-squares misfit χ^2 divided by the degrees of freedom) and model fit (Fig. 5c) and unless otherwise noted is used hereafter to explore the bounds on the best-fitting model.

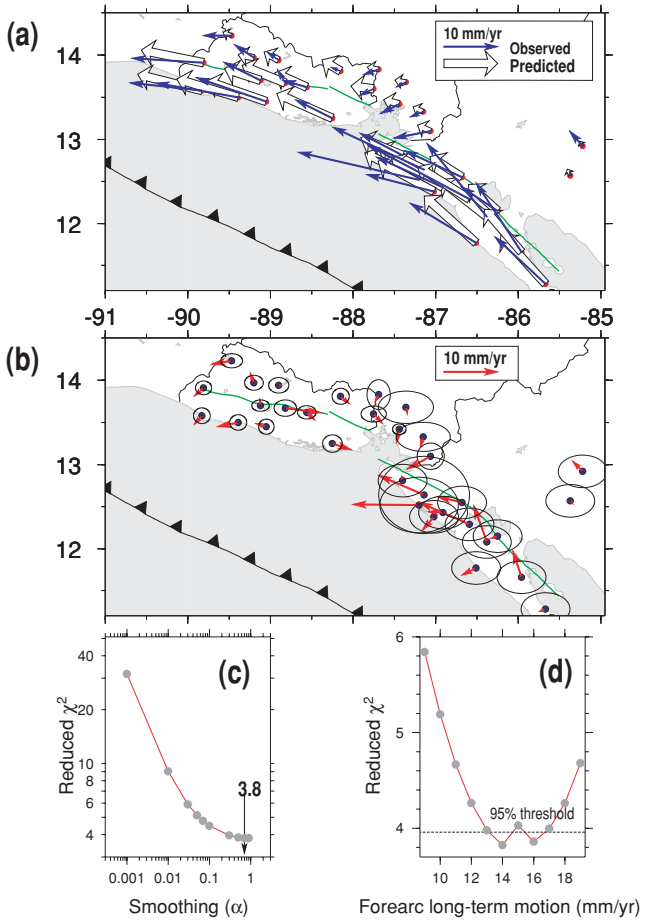

Figure 5. (a) Observed GPS station velocities (blue) and velocities predicted by the best-fitting inverse model (open). Caribbean plate is fixed. (b) Residual velocities (red arrows) and 2-D, 1σ velocity uncertainty ellipses relative to best-fitting model predictions. (c) Variation in fit to the GPS velocity field as a function of the coefficient (α) that is used to smooth the best-fitting distributions of volcanic arc fault and subduction interface coupling shown in Fig. 7. Long-term forearc motion of 14 mm yr^{-1} is assumed for this model and is based on results shown in (d). The best-fitting model has a smoothing coefficient of 0.7, corresponding to reduced χ^2 of 3.8. (d) Variation in fit versus forearc slip rate. Dashed horizontal line shows 95 per cent limits for the slowest and fastest long-term slip rate based on a F-ratio comparison of the best-fitting value for reduced χ^2 (3.8) relative to values for the alternative slip rates.

4.1 Long-term forearc slip rates

Long-term forearc slip rates of 14 and 16 mm yr^{-1} (Fig. 5d) give equally low values for reduced chi-square (χ^2_ν). These rates agree well with independently estimated slip rates from plate kinematic data (DeMets 2001), geomorphologic observations (Corti *et al.* 2005), and GPS velocities (Turner *et al.* 2007; Alvarado 2008). The coupling distributions across both the volcanic arc faults and subduction interface are nearly the same for both of these long-term slip rates. Consequently, none of the results or conclusions below are depend significantly on which of the two slip rates we adopt. Below, we adopt the 14 mm yr^{-1} rate, which agrees with that determined by Alvarado (2008).

As part of a related analysis (Alvarado *et al.*, 'Forearc motion and deformation between El Salvador and Nicaragua', in preparation 2009), we examine whether the fits to the velocities for GPS stations from the Salvadoran and Nicaraguan forearcs improve significantly

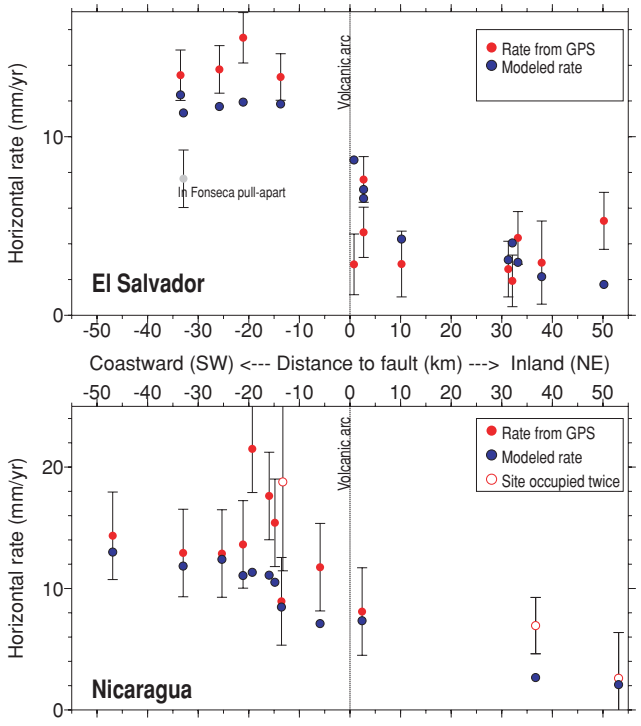

Figure 6. Components of observed (red) and modelled (blue) GPS station rates parallel to volcanic arcs of El Salvador (upper) and Nicaragua (lower) as a function of station distance from the volcanic arcs. The poor fit to the velocity of the station located in the Fonseca pull-apart zone is likely caused by deformation within the Salvadoran forearc in this region (Alvarado 2008). Uncertainties are 1σ. Stations are collapsed onto arc-perpendicular profiles.

if we estimate separate long-term slip rates for the two forearcs. Although Alvarado *et al.* find that the fit to the GPS velocities is improved when the Nicaraguan forearc is permitted to move somewhat more rapidly (17 mm yr^{-1}) than the Salvadoran forearc (14 mm yr^{-1}), the improvement in fit is not significant at a high (99 per cent) confidence level relative to the fit for a model in which both forearcs are required to move at the same rate. Significant motion between the two forearcs thus cannot be resolved with the present GPS velocities. We therefore adopt a single forearc model below.

4.2 Fits to GPS station velocities

The best-fitting model matches the pattern in the observed velocity field (Figs 5a and 6), with average misfits of 1.7, 2.7 and 4.4 mm yr^{-1} for the north, east and vertical components of the station velocities, respectively. The well-determined velocities of most sites in El Salvador are fit close to the level of their estimated uncertainties. The misfits for the Nicaraguan station velocities are somewhat larger than for the Salvadoran stations (Figs 5a and 6), most likely because some of the Nicaraguan stations have shorter time-series with fewer occupations and less data per occupation than for the Salvadoran sites. The imperfectly known elastic corrections for the coseismic offsets that occurred at the Nicaraguan sites during the 2001 January 13 El Salvador earthquake may also degrade the fit.

Several misfits to individual station velocities merit mention. The best-fitting model underestimates by 1–2 mm yr^{-1} the measured rates for four of the five Salvadoran stations outboard from the volcanic arc (Fig. 6), indicating that the model predicts slower long-term forearc motion than is observed. These misfits are most likely caused by trade-offs in the fit between the estimated long-term forearc slip rate and the estimated depth and degree of coupling for the volcanic arc faults. Our best-fitting model overestimates by 4 mm yr^{-1} the motion of a station (JUCU) from an area of southeastern El Salvador (Fig. 5b) where distributed east–west extension associated with the Fonseca pull-apart basin (Alvarado 2008) may bias the station motion estimate. Finally, the best-fitting model overestimates by 6 mm yr^{-1} the motion of one slowly moving station (DERA) that is located close to the El Salvador fault zone along the volcanic arc (Fig. 6). This misfit and possibly others for stations near or within the volcanic arc might be evidence that some sites are caught within localized fault stepovers and thus may not record the full motion of the forearc or areas inland from the volcanic arc.

Reduced chi-square for our best-fitting model is 3.8, indicating that the site velocities are misfit on average by nearly twice their assigned uncertainties. The higher-than-expected misfit might be caused by velocity uncertainties that are too small, by one or more of the assumptions we employ for our model, or by our relatively simple FEM representation of the geometry of the volcanic arc faults. For example, numerical experiments indicate that our assumption that the Salvadoran and Nicaraguan forearcs move as a single sliver increases the squared misfit by ∼7 per cent, accounting for some of the higher-than-expected misfit. Our assumption that stations inland from the volcanic arc move with the Caribbean Plate interior is also only approximate given that slow extension occurs in areas of Honduras north of the Salvadoran volcanic arc (Rodriguez *et al.* 2009). Each of these constitutes an area for future work once the geographic coverage and uncertainties in the GPS velocities improve enough to merit the effort.

4.3 Coupling of the subduction interface

Our best-fitting solution indicates that the degree of coupling across the subduction interface averages only ∼2 per cent over the modelled area (Fig. 7b), with evidence for an absence of any coupling in most areas offshore. One area of higher coupling lies offshore from southeastern Nicaragua, where coupling is as high as ∼25 per cent and extends downdip to depths of 40–50 km. Just southeast of this area of moderately higher coupling, Norabuena *et al.* (2004) find evidence for 50 per cent or greater coupling across the subduction interface at depths of 11–18 km beneath the Nicoya Peninsula of Costa Rica. There may thus be a gradual transition in the strength of the interseismic coupling between the Nicoya peninsula and areas offshore from western Nicaragua and El Salvador. We are presently extending our mesh and analysis to include GPS velocities from adjacent areas of Costa Rica in order to test this hypothesis and determine whether the transition is gradual or more sudden.

Our best-fitting model also includes a weakly locked patch offshore from central El Salvador, where coupling of up to ∼10 per cent may occur between depths of 30 and 60 km on the subduction interface (Fig. 7b). We next exploit features of the bounded-variable inverse technique to evaluate whether this patch and other features of the best-fitting coupling distribution are well resolved by the data.

4.3.1 Sensitivity analyses of subduction coupling

Below, we address two questions about our best-fitting estimate of subduction coupling. We first examine how much coupling might occur across the subduction interface without violating the

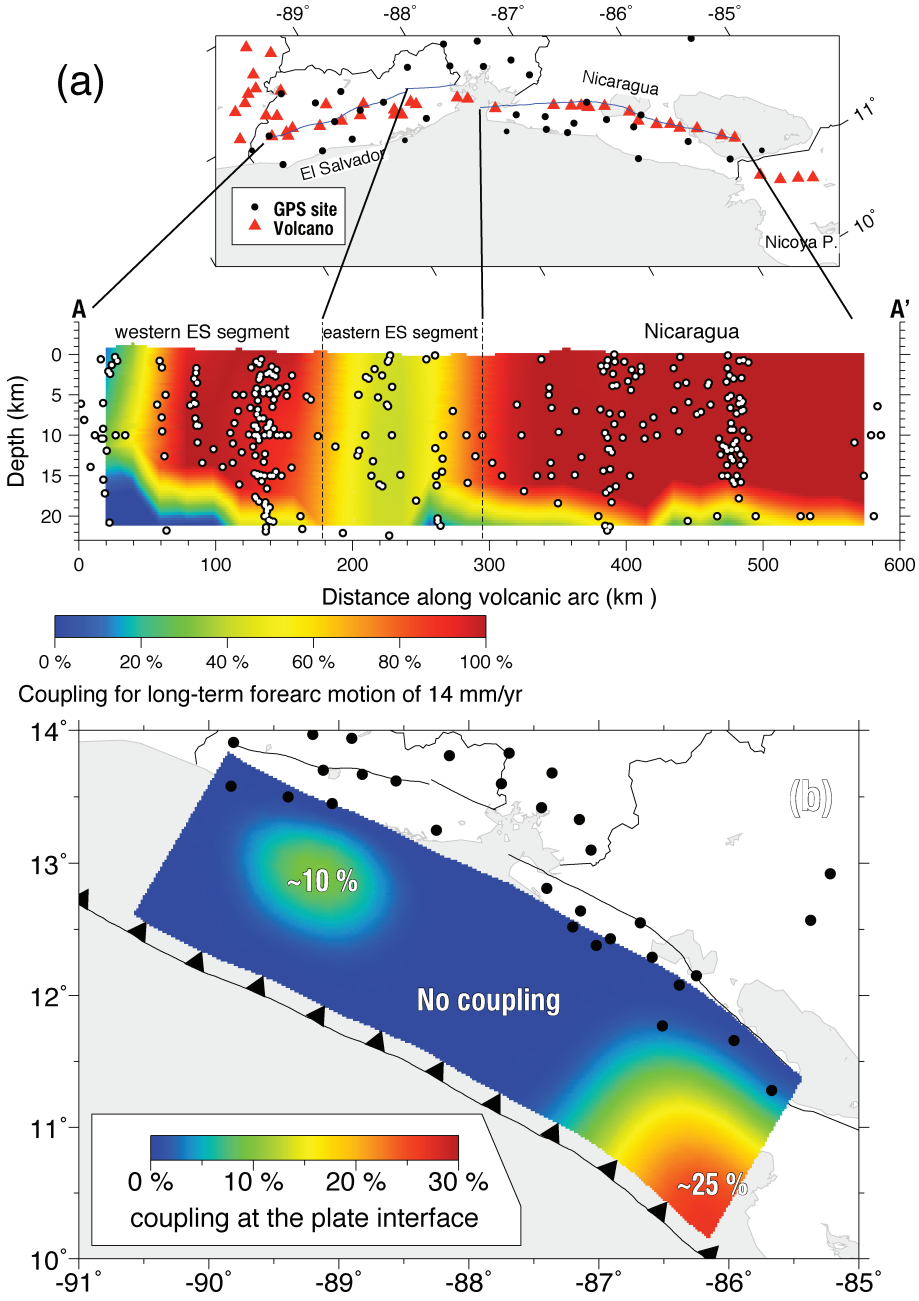

Figure 7. Best-fitting inverse models for distribution of interseismic coupling for (a) faults in the volcanic arc and (b) the subduction interface. Uppermost panel is an oblique Mercator projection of the study area corresponding to the profile shown in Fig. 3(b). Bold lines indicate endpoints of the three volcanic arc fault segments. Red triangles in upper panel show locations of volcanos that have been active in the Quaternary, and black circles show GPS station locations. White circles in (a) are relocated earthquake hypocentres (Engdahl *et al.* 1998) from a 50-km-wide zone centred on the volcanic arc.

constraints imposed by our GPS velocity field. As part of this analysis, we also estimate the distribution of coupling for two models in which the region of permitted coupling is limited to shallower parts of the subduction interface. We then determine whether the weakly locked patches off the coasts of southeastern Nicaragua and central El Salvador are well resolved by the data.

An upper limit for the average degree of coupling: To determine whether the spatially averaged degree of coupling for subduction interface nodes above a depth of 100 km might be significantly higher than the 2 per cent average implied by our best-fitting coupling distribution, we incrementally increased the lower permitted bound for the coupling coefficient from 1 per cent to 30 per cent to find how χ^2_ν varies as a function of the lowest permitted coupling coefficient (Fig. 8a). Our inversions of the data for each assumed lower coupling bound employ the same smoothing coefficient as for our best-fitting solution to ensure that changes in χ^2_ν are caused solely by changes in the lower coupling bound that is assumed for each inversion.

The misfit χ^2_ν increases rapidly as a function of the enforced lower coupling limit (Fig. 8a), thereby indicating that the average degree of coupling is well resolved by the data. Relative to the best-fitting solution, the increase in the misfit is significant at the 95 per cent confidence level for all inversions for which a lower coupling bound of 3 per cent or more is enforced (Fig. 8a). The spatially averaged

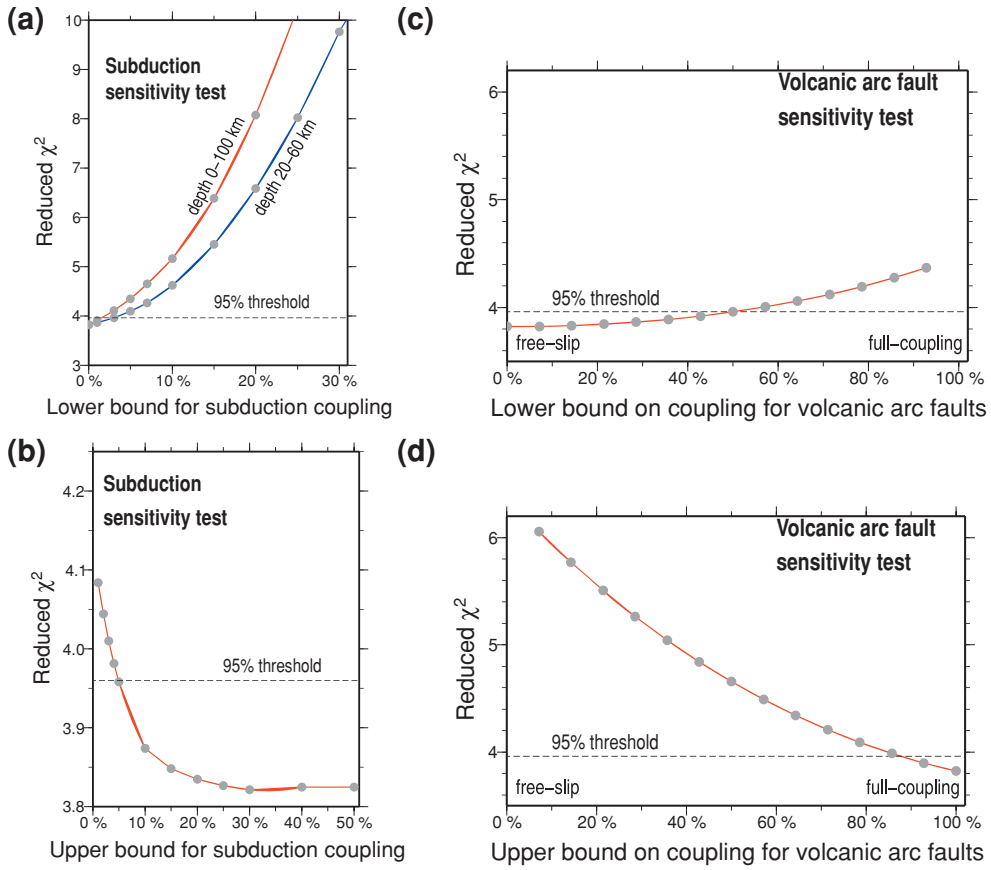

Figure 8. (a) Variation in fit to GPS station velocities as a function of the lower enforced bound for the coupling value at each subduction interface node within our bounded value inversion for permitted coupling areas that extend from the trench to 100 km (red curve) and from 20 to 60 km (blue curve). Value for 10 per cent corresponds to fit for an inversion in which the coupling value per node was not permitted to drop below 10 per cent. Dashed horizontal lines in (a)–(d) show the 95 per cent fit threshold from an *F*-ratio test. Models with reduced chi-square above the threshold give unacceptable fits to the data. (b) Variation in fit as a function of the maximum enforced bound for the coupling value at each subduction interface node. In this case, a value of 10 per cent corresponds to the fit for an inversion in which the coupling value per node was not permitted to exceed 10 per cent. (c) Variation in fit as a function of the lower enforced bound for the coupling value at each volcanic arc fault node. Value for 10 per cent corresponds to fit for an inversion in which the coupling value per node was not permitted to drop below 10 per cent. (d) Variation in fit as a function of the upper enforced bound for the coupling value at each volcanic arc fault node. Value for 90 per cent corresponds to fit for an inversion in which the coupling value per node was not permitted to exceed 90 per cent.

coupling coefficient down to a depth of 100 km can thus be no higher than 2 per cent without significantly misfitting the data.

Most of the thrust faulting earthquakes in this region occur between depths of 20 and 60 km (Fig. 2b) rather than to depths of 100 km, as is assumed above. We thus repeated the above analysis while restricting the nodes that can acquire non-zero coupling values to depths of 20–60 km. Doing so gives an upper limit of only 3 per cent for the average degree of coupling (blue curve in Fig. 8a). The degree of coupling is thus weak even if we use a smaller, potentially seismogenic region for our model.

Coupling above 20 km: LaFemina *et al.* (2009) propose that coupling offshore from Nicaragua may be limited to depths shallower than 20 km, corresponding to the apparent rupture limit of the M_s 7.2, 1992 September 2 Nicaragua tsunamigenic earthquake off the coast of southeastern Nicaragua (Satake 1994). Detecting coupling at the upper limits of the subduction interface is challenging due to its remoteness from the onland GPS network, but is potentially important since shallow ruptures can generate destructive tsunamis. We thus use forward and inverse modelling below to examine whether the GPS velocities provide any information about possible coupling at the shallowest levels of the subduction interface offshore from El Salvador and Nicaragua.

We first test a forward model in which the subduction interface nodes below 20-km depth are uncoupled and the nodes above 20 km are fully coupled and accumulate an annual elastic slip deficit equal to the full Cocos–Caribbean Plate convergence rate. This model predicts that GPS stations along the coasts of El Salvador and Nicaragua should move inland at respective rates of 3 and 3–5 mm yr^{-1}. In contrast, the observed velocities show no evidence for any inland component of motion (Fig. 1b). Within their $\pm$1–2 mm yr^{-1} uncertainties, the Salvadoran GPS velocities exclude a model in which the subduction interface offshore from El Salvador is uniformly, fully coupled at depths shallower than 20 km. The Nicaraguan velocity uncertainties are too large to exclude such a model (Table 1), although the sites along the Nicaraguan coast do not exhibit any inland motion indicative of shallow strain accumulation. The velocity uncertainties in both countries are too large to exclude the possibility that isolated, fully coupled patches exist above depths of 20 km, provided that the spatially averaged coupling of the interface above 20 km is not greater than ~30–50 per cent.

An inversion of the GPS velocities in which non-zero coupling is limited to depths above 20 km yields coupling values of 5 per cent or less at the individual nodes offshore from El Salvador and western Nicaragaua and coupling of 60–70 per cent within a

shallow, elongate patch located offshore from southeastern Nicaragua. The data are thus consistent with partial coupling of the subduction interface above depths of 20 km off the coast of southeastern Nicaragua, in agreement with results reported by LaFemina *et al.* (2009) based on inversions of velocities from GPS stations in Costa Rica and Nicaragua. Both our own and LaFemina's analyses however indicate that coupling offshore from southeastern Nicaragua is partial, possibly indicating that even the shallow regions of the subduction interface consist of strongly locked patches surrounded by weakly coupled zones.

Resolvability of weakly locked patches: We tested how well the weakly locked patches offshore from El Salvador and Nicaragua are resolved by comparing the fits of models in which all coupling values are required to be smaller than the maximum degree of coupling across the weakly locked patches offshore from Nicaragua (∼25 per cent) and El Salvador (∼10 per cent). We accomplished this by examining the variation in fit as a function of progressively smaller upper bounds on the permitted degree of coupling.

For upper bounding values that exceed 30 per cent, χ^2_ν differs insignificantly from the best-fitting solution (Fig. 8b), as expected given that none of the nodes in the locked patches offshore from El Salvador or southeastern Nicaragua have coupling values that exceed ∼25 per cent. The misfit does not increase significantly (i.e. at the 95 per cent confidence level) until coupling is not permitted to exceed 4 per cent at any node. The weakly locked patches offshore from Nicaragua and El Salvador are thus only poorly resolved by our data, which are fit nearly as well if we impose more homogeneous coupling (0–4 per cent) on the solution.

Summary of sensitivity results: Models in which coupling everywhere along the subduction interface is required to exceed 3 per cent of the plate convergence rate are strongly excluded by the available GPS velocities, thereby indicating that coupling across the subduction interface is weak or absent in most areas. Possibly stronger coupling may occur offshore from southeastern Nicaragua, particularly at depths above 20 km; however, both of the partially coupled patches in our best-fitting model are poorly resolved.

4.4 Volcanic arc fault coupling and long-term forearc motion

The spatially averaged coupling across faults in the volcanic arcs of Nicaragua and El Salvador is more than ∼80 per cent (Fig. 7a), suggesting that faults in both volcanic arcs are nearly fully locked. In central and western El Salvador, where the well-defined El Salvador fault zone defines the inland edge of the forearc sliver, the estimated coupling remains strong from the surface to depths of 15–20 km. Our results are consistent with the occurrence of large strike-slip earthquakes such as the M_w 6.6 2001 February 13 earthquake along the El Salvador fault zone (Martinez-Diaz *et al.* 2004) and with relocated earthquake hypocentres (Engdahl *et al.* 1998) that extend to depths of 15–20 km along the volcanic arc (Fig. 7a). Volcanic arc earthquakes located by the Salvadoran national seismic network (SNET) and earthquakes in the Gulf of Fonseca located by the Nicaraguan agency INETER also extend to depths of 15–20 km (not shown).

Fault coupling in Nicaragua also appears to be strong to depths of 18–20 km (Fig. 7a). Given that narrow forearc-bounding faults are generally absent in Nicaragua (La Femina *et al.* 2002; Funk *et al.* 2009), we interpret the strong coupling as evidence that faults in the volcanic arc, including faults that trend transverse to the arc, strongly resist the dextral northwestward motion of the forearc.

The only notable variation in coupling along the length of the volcanic arc coincides with the fault segment in eastern El Salvador, where coupling values are only 40–50 per cent (Fig. 7a). Contours of the model resolution values for the volcanic arc fault nodes however show that coupling along this part of the volcanic arc is more poorly resolved than elsewhere in the study area, most likely because the GPS stations in this region are more distant from the volcanic arc faults and are primarily located inland. In addition to the low model resolution in this area, deformation in eastern El Salvador is not limited solely to faults in the volcanic arc, as is assumed in our FEM, but instead occurs within a broad extensional zone in eastern El Salvador and the Gulf of Fonseca (Alvarado 2008). We therefore consider the lower coupling estimate for eastern El Salvador to be unreliable.

4.4.1 *Sensitivity analysis for volcanic arc fault coupling*

We determined a minimum spatially averaged coupling value for the volcanic arc faults by inverting the GPS velocities for a series of models in which we progressively decreased the maximum degree of coupling permitted at each volcanic arc fault node (Fig. 8d). All inversions in which we enforce a maximum coupling bound that is smaller than 85 per cent fit the data significantly more poorly than does the best-fitting model. The data thus require that the spatially averaged coupling along the volcanic arc faults is 85 per cent or higher.

Many of the nodes at depths of ∼20 km have coupling values that are unexpectedly high for a presumably hot and rheologically weak volcanic arc (Fig. 7a). We therefore tested whether the misfit χ^2_ν increases significantly if we re-invert the data while requiring all coupling to occur at depths shallower than 20 km. When non-zero coupling is limited to depths of ∼10 km or shallower, χ^2_ν is 50 per cent higher than for the best-fitting solution. The increase in misfit is highly significant, indicating that some coupling occurs below 10 km. We also inverted the data while limiting coupling to depths of 8–15 km, but found that this also significantly increases the misfit. Because the volcanic arc faults are represented in our FEM with nodes at only four depths, a more detailed examination of the possible upper and lower limits of coupling along these faults was not possible. Measurements at additional sites and modelling with a denser concentration of volcanic arc fault nodes are needed for an improved understanding of coupling along the arc.

5 DISCUSSION AND CONCLUSIONS

We next discuss the implications of our results for seismic hazard and deformation along the western edge of Central America, beginning with an interpretation of our results in the context of previously published studies of the degree of seismic coupling based on the recent and historic record of large earthquakes in Central America.

5.1 Reconciling geodetic and seismic estimates of subduction interface coupling

Our geodetic evidence for weak interseismic coupling across large parts of the subduction interface offshore from El Salvador and western Nicaragua (Fig. 9) strongly supports previous inferences of a large seismic slip deficit in this region based on the earthquake record over the past century (McNally & Minster 1981; Pacheco *et al.* 1993; Guzman-Speziale & Gomez-Gonzalez 2006). Our results are however inconsistent with the conclusion reached by White

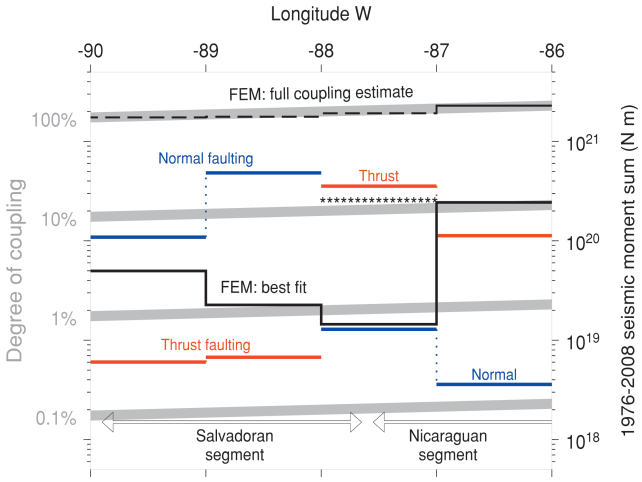

Figure 9. Summed global centroid moment tensor moments for subduction interface thrust (red) and normal (blue) faulting earthquakes, 1976–2008, versus the estimated moment accumulation for the same period from our FEM. Two FEM estimates are shown, one for full (100 per cent) coupling at the plate convergence rate of all subduction interface nodes from the trench to a depth of 60 km, and the other for our best-fitting coupling estimate (Fig. 7b). The FEM-estimated and seismic moments are binned and summed per degree of longitude. Grey areas indicate equivalent degrees of coupling. Asterisks show the seismic moment of the M_w 7.6 1992 September 2 Nicaragua tsunami earthquake.

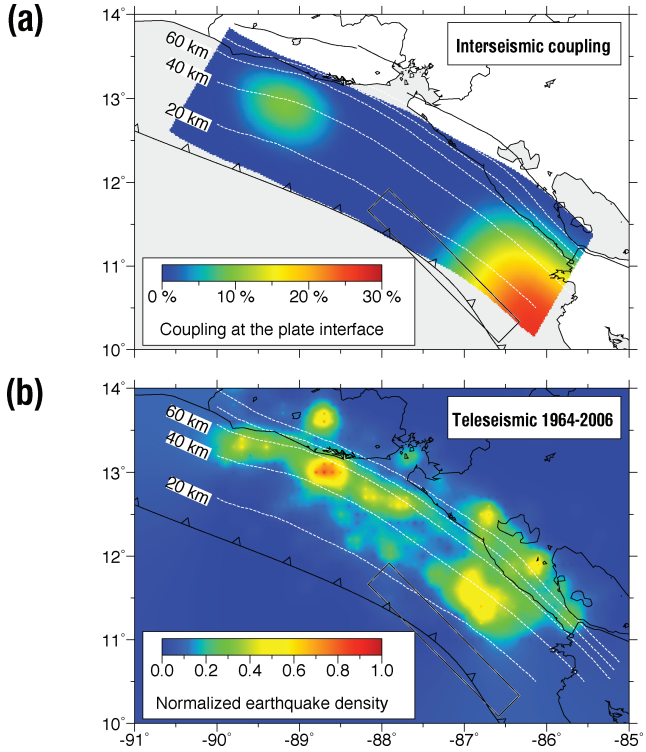

Figure 10. (a) Comparison of interseismic coupling distribution from Fig. 7(b) to earthquake densities shown in (b). Earthquake density is defined to be the number of teleseismic earthquakes of all magnitudes that are located within adjacent ∼120 km^2 regions (0.1° squares), normalized by the maximum count for the study region. White dashed lines are subduction depth contours from Fig. 1(a). (b) Earthquake density for all events in the study area from 1964 to 2006 (Fig. 1a) after removing aftershocks within 3 months of the 1982 June 19 and 2001 January 13 intraslab normal faulting earthquakes. Grey box shows rupture area for the 1992 M_w 7.6 Nicaragua tsunami earthquake (Satake 1994).

et al. (2004) that as much as 60 ± 10 per cent of the cumulative plate convergence since 1690 has been accommodated by downdip rupture along the subduction interface.

Two factors may contribute to the discrepancy between our geodetically derived and White *et al.*'s seismologically based estimates. First, many of the pre-instrumental offshore earthquakes that White *et al.* use to estimate the cumulative seismic slip since 1690 may have originated within the subducting slab instead of along the subduction interface. Their estimate may therefore significantly overstate the amount of seismic slip along the subduction interface. Alternatively, the degree of coupling might vary with time. We briefly discuss each possibility below.

The recent earthquake history of areas offshore from El Salvador provides the best evidence that normal faulting earthquakes within the subducting Cocos Plate may comprise some or possibly most of the destructive, historic offshore earthquakes that were provisionally identified by White *et al.* as thrust faulting events. Over the past few decades, only two large earthquakes have occurred offshore from El Salvador, one on 1982 June 19 (M_w 7.3) and the other on 2001 January 13 (M_w 7.7). Both were intraslab normal faulting earthquakes (Fig. 2c). As was recognized by White *et al.*, pre-instrumental accounts of earthquake damage offer no way to discriminate between thrust faulting earthquakes along the subduction interface and offshore earthquakes within the subducting slab. Any pre-instrumental earthquakes described by White *et al.* that were large normal-faulting, intraslab events would have upward-biased their seismic slip estimate relative to its true value.

Alternatively, large intraslab normal-faulting earthquakes might alter the orientations and magnitudes of the stresses that act on the subduction interface and hence may induce variations in both time and space in the degree of coupling across the subduction interface. The cumulative seismic moments for intraslab normal faulting earthquakes and subduction thrust earthquakes offshore from El Salvador and Nicaragua from 1976 to 2008 (Fig. 9) weakly support such a hypothesis, with little thrust faulting observed to occur in areas where large intraslab normal faulting earthquakes occur and more thrust faulting in areas where large intraslab earthquakes have not occurred. Modelling of how a normal faulting earthquake within the subducting slab alters the Coulomb failure stresses across the nearby subduction interface is needed to test the plausibility of this hypothesis.

5.2 Subduction interface: seismic gap interpretation

A map of the density of earthquake epicentres in the study area (Fig. 10b) clearly displays the absence of shallow earthquakes that has been noted by previous authors (e.g. McNally & Minster 1981; Pacheco *et al.* 1993; Dewey *et al.* 2004). In contrast to other parts of the Middle America trench, most earthquakes offshore from El Salvador and northwestern Nicaragua are concentrated in a narrow band between the 40- and 60-km slab-depth contours, where intense intraslab normal faulting occurs (Fig. 2bc).

The geodetic evidence described above for weak coupling offshore from El Salvador and western Nicaragua suggests that the low rate of elastic strain energy accumulation is responsible for the seismic gap and seismic slip deficit in those areas. The available data do not lend themselves to a more classic seismic gap interpretation in which the absence of microseisms is associated with an enhanced probability for future large earthquakes based on the presumption of a strongly coupled subduction interface. Our

geodetic data do not preclude the existence of isolated, strongly coupled patches above depths of 20 km offshore from El Salvador and western Nicaragua, mainly because the elastic signature of small strongly coupled patches would be too small to detect at land-based sites given the remoteness of the GPS sites from the trench, the wide spacing between many of the coastal GPS stations, and the prevailing GPS velocity uncertainties.

In contrast to the absence of shallow earthquakes offshore from El Salvador and northwestern Nicaragua, thrust faulting earthquakes and earthquake epicentres offshore from southeastern Nicaragua extend up dip to the 20-km-depth contour (Figs 2b and 10bc) and the tsunamigenic Nicaragua earthquake in 1992 ruptured the subduction interface from a depth of 20 km to the surface (Satake 1994). The subduction interface in this region is thus more obviously seismogenic. Our analysis also suggests that interseismic coupling is higher offshore from southeastern Nicaragua than elsewhere in the study area (Fig. 7b), reaching values of 60–70 per cent if we limit coupling to areas of the subduction interface shallower than 20 km and 25 per cent for inversions where coupling is permitted to occur to depths of 100 km. The degree of coupling offshore from southeastern Nicaraguan is still poorly resolved, although the seismic and geodetic evidence favour enhanced coupling in the upper 20 km of the subduction interface. Future estimates of interseismic coupling in this region should benefit significantly from improved estimates of the Nicaraguan station velocities and additional constraints from GPS station velocities in nearby Costa Rica (LaFemina *et al.* 2009).

5.3 Volcanic arc faults: coupling estimates

Our best-fitting coupling distribution for faults in the volcanic arc (Fig. 7a) indicates that coupling across the volcanic arc faults is 85–100 per cent in most areas and extends to depths of ∼20 km. Significant misfits to the data occur if we force the average coupling to values lower than 85 per cent (Fig. 8c). Strong coupling for the volcanic arc faults is thus a robust aspect of our analysis. Our results agree with the historically high level of earthquake activity in the volcanic arc (Fig. 1 and White & Harlow 1993) and with evidence that earthquakes extend to depths of 15–20 km along the volcanic arc (Fig. 7a).

Two factors introduce some uncertainty into our estimate of volcanic arc fault coupling. First, areas of Honduras and possibly El Salvador inland from the volcanic arc undergo active east–west extension (Rodriguez *et al.* 2009) that is not explicitly modelled in our FEM. We assessed whether such deformation might affect our estimate of coupling across the volcanic arc faults by re-inverting the GPS velocities after removing all station velocities from areas of El Salvador and Honduras that may be affected by this extension. The modified distribution of fault coupling (not shown) strongly resembles that for our best-fitting model. Our best fitting model is thus robust with respect to any slow extension inland from the volcanic arc.

Our assumption that the Nicaraguan and Salvadoran forearcs move together as a single, elastically deforming sliver also introduces uncertainty into the coupling estimates shown in Fig. 7(a) via the trade-off in fit that exists between the estimated degree of fault coupling and the estimated long-term rate of forearc motion. Alvarado (2008) finds that stations in the Nicaraguan forearc move somewhat faster (16 ± 2 mm yr^{-1}) than do the Salvadoran forearc sites (14 ± 1 mm yr^{-1}) and that as much as 3 mm yr^{-1} of trench-parallel shortening within the forearc could occur within the GPS site velocity uncertainties. If future GPS measurements demonstrate that the forearc deforms slowly, then the long-term slip rates for the two forearcs will have to be estimated separately during an inversion for the distribution of coupling across the faults in the Nicaraguan and Salvadoran volcanic arcs.

Measurements at additional sites on the forearc and along the volcanic arc are now being made by ourselves and other groups to provide a stronger basis for more detailed estimates of coupling across faults in the volcanic arc. Of particular interest is whether creep occurs anywhere along strike and whether fault coupling might be locally influenced by stress perturbations related to nearby volcanos, as proposed by Cailleau *et al.* (2007). The influence of extensional fault stepovers, where one or more normal faults transfer motion between the tips of active, offset strike-slip faults, is also poorly understood and is a target of ongoing measurements.

5.4 Tectonic implications

DeMets (2001) postulates that oblique Cocos–Caribbean Plate convergence offshore from southeastern Nicaragua is partitioned into trench-parallel and trench-normal components, the former of which drives the long-term northwest motion of the Nicaraguan forearc. Partitioning however cannot be invoked to explain the similarly rapid trench-parallel movement of the Salvadoran forearc because the direction of Cocos–Caribbean convergence offshore from El Salvador is orthogonal to the trench within uncertainties (Alvarado 2008). It is thus puzzling why the two forearcs have nearly the same trench-parallel rates of motion (Fig. 6).

One possible explanation for this conundrum is that the northwestward motion of the Nicaraguan forearc in response to partitioning of oblique convergence beneath southeastern Nicaragua (DeMets 2001) pushes the Salvadoran forearc to the northwest. Weak coupling across the subduction interface offshore from El Salvador may facilitate this process. Alternatively, LaFemina *et al.* (2009) hypothesize that the collision of the oceanic Cocos ridge offshore from Costa Rica may cause northwestward movement of the Costa Rican, Nicaraguan, and Salvadoran forearcs. Our results are also consistent with LaFemina *et al.*'s hypothesis, although they do not constitute a test of that hypothesis.

ACKNOWLEDGMENTS

The first author is grateful to CONACYT for scholarship support during his research at the University of Wisconsin. We thank Pete LaFemina, Laura Wallace and John Beavan for their constructive reviews and thank Servicio Nacional de Estudios Territoriales of El Salvador, Universidad Nacional Autonoma de Honduras and COPECO of Honduras for logistical support. This work was funded by NSF grants EAR-0309839 and EAR-0538131 (DeMets) and EAR-0085432 (Mattioli). Figures were produced using Generic Mapping Tools software (Wessel & Smith 1991).

REFERENCES

Agostini, S. *et al.,* 2006. Tectonic and magmatic evolution of the active volcanic front in El Salvador: insight into the Berlin and Ahuachapan geothermal areas, *Geothermics,* **35,** 368–408, doi:10.1016/j.geothermics.2006.05.003.

Altamimi, Z., Collilieux, X., Legrand, J., Garayt, B. & Boucher, C., 2007. ITRF2005: a new release of the International Terrestrial Reference Frame based on time series of station positions and Earth orientation parameters, *J. geophys. Res.,* **112,** B09401, doi:10.1029/2007JB004949.

Alvarado, D., 2008. Crustal deformation of the Salvadoran-Nicaraguan forearc at the Gulf of Fonseca: a multidisciplinary tectonic study, *M. S. thesis*, 113 pp., University of Wisconsin-Madison.

Alvarez-Gomez, J.A., Meijer, P.T., Martinez-Diaz, J.J. & Capote, R., 2008. Constraints from finite element modeling on the active tectonics of northern Central America and the Middle America Trench, *Tectonics,* **27,** TC1008, doi:10.1029/2007TC002162.

Bassin, C., Laske, G. & Masters, G., 2000. The current limits of resolution for surface wave tomography in North America, *EOS Trans. AGU,* **81**(48), Fall Meeting Suppl., Abstract S12A-03.

Benito, B., Cepeda, J.M. & Martinez-Diaz, J.J., 2004. Analysis of the spatial and temporal distribution of the 2001 earthquakes in El Salvador, in *Natural Hazards in El Salvador,* Vol. 375, pp. 339–356, eds Rose, W.I., Bommer, J.J.L., Lopez, D., Carr, M.J. & Major, J.J., Geol. Soc. Am. Spec. Pap., The Geological Society of America, Boulder.

Bommer, J. *et al.,* 2002. The Salvador earthquakes of January and February 2001: context-characteristics and implications for seismic risk, *Soil Dyn. Earthq. Eng.,* **22,** 389–418.

Burbach, G.V., Frohlich, C., Pennington, W.D. & Matumoto, T., 1984. Seismicity and tectonics of the subducted Cocos plate, *J. geophys. Res.,* **89,** 7719–7735.

Cailleau, B., LaFemina, P.C. & Dixon, T.H., 2007. Stress accumulation between volcanoes: an explanation for intra-arc earthquakes in Nicaragua? *Geophys. J. Int.,* **169**(3), 1132–1138, doi:10.1111/j.1365-246X.2007.03332.x.

Correa-Mora, F., DeMets, C., Cabral-Cano, E., Marquez-Azua, B. & Diaz-Molina, O., 2008. Interplate coupling and transient slip along the subduction interface beneath Oaxaca, Mexico, *Geophys. J. Int.,* **175,** 269–290, doi:10.1111/j.1365-246X.2008.03910.x.

Corti, G., Carminati, E., Mazzarini, F. & Garcia, M.O., 2005. Active strike-slip faulting in El Salvador, Central America, *Geology,* **33,** 989–992.

Cowan, H., Prentice, C., Pantosti, D., de Martini, P., Strauch, W. & Workshop, Participants, 2002. Late Holocene earthquakes on the Aeropuerto fault, Managua, Nicaragua, *Bull. seism. Soc. Am.,* **92,** 1694–1707.

DeMets, C., 2001. A new estimate for present-day Cocos-Caribbean plate motion: implications for slip along the Central American volcanic arc, *Geophys. Res. Lett.,* **28,** 4043–4046.

DeMets, C., Mattioli, G., Jansma, P., Rogers, R., Tenorio, C. & Turner, H.L., 2007. Present motion and deformation of the Caribbean plate: constraints from new GPS geodetic measurements from Honduras and Nicaragua, in *Geologic and Tectonic Development of the Caribbean Plate in Northern Central America,* pp. 21–36, ed. Mann, P., Geol. Soc. Am. Spec. Paper 428, The Geological Society of America, Boulder, doi:10.1130/2007.2428(02).

Dewey, J.W., White, R.A. & Hernandez, D.A., 2004. Seismicity and tectonics of El Salvador in *Natural Hazards in El Salvador,* Vol. 375, pp. 363–378, eds Rose, W.I., Bommer, J.J.L., Lopez, D., Carr, M.J. & Major, J.J., Geol. Soc. Am. Spec. Pap., The Geological Society of America, Boulder.

Engdahl, R.E., van der Hilst, R. & Buland, R., 1998. Global teleseismic earthquake relocation with improved travel times and procedures for depth determination, *Bull. seism. Soc. Am.,* **88,** 722–743.

Fournier, T.J. & Freymueller, J.T., 2007. Transition from locked to creeping subduction in the Shumagin region, Alaska, *Geophys. Res. Lett.,* **34,** L06303, doi:10.1029/2006GL029073.

Funk, J., Mann, P., McIntosh, K. & Stephens, J., 2009. Cenozoic tectonics of the Nicaraguan depression, Nicaragua, and Median trough, El Salvador, based on seismic reflection profiling and remote sensing data, *Geol. soc. Am. Bull.,* B26512.1, doi:10.1130/B26512.1.

Guzman-Speziale, M. & Gomez-Gonzalez, J.M., 2006. Seismic strain rate along the Middle America trench reveals significant differences between Cocos-North America and Cocos-Caribbean convergence, *Geophys. J. Int.,* **166,** 179–185.

La Femina, P.C., Dixon, T.H. & Strauch, W., 2002. Bookshelf faulting in Nicaragua, *Geology,* **30,** 751–754.

LaFemina, P.C. *et al.,* 2009. Forearc motion and Cocos Ridge collision in Central America, *Geochem. Geophys. Geosys.,* **10,** Q05S14, doi:10.1029/2008GC002181.

Lay, T. & Schwartz, S., 2004. Comment on 'Coupling semantics and science in earthquake research', *EOS, Trans. Am. geophys. Un.,* **85,** 339–340.

Lyon-Caen, H. *et al.,* 2006. Kinematics of the North American-Caribbean-Cocos plates in Central America from new GPS measurements across the Polochic-Motagua fault system, *Geophys. Res. Lett.,* **33,** L19309, doi:10.1029/2006GL027694.

Martinez-Diaz, J.J., Alvarez-Gomez, J.A., Benito, B. & Hernandez, D., 2004. Triggering of destructive earthquakes in El Salvador, *Geology,* **32,** 65–68, doi:10.1130/G20089.1.

McNally, K.C. & Minster, J.B., 1981. Nonuniform seismic slip rates along the Middle America Trench, *J. geophys. Res.,* **86,** 4949–4959.

Molnar, P. & Sykes, L.R., 1969. Tectonics of the Caribbean and Middle America regions from focal mechanisms and seismicity, *Bull. seism. Soc. Am.,* **80,** 1639–1684.

Norabuena, E. *et al.,* 2004. Geodetic and seismic constraints on some seismogenic zone processes in Costa Rica, *J. geophys. Res.,* **109,** B11403, doi:10.1029/2003JB002931.

Okada, Y., 1985. Surface deformation due to shear and tensile faults in a half-space, *Bull. seism. Soc. Am.,* **75,** 1135–1154.

Pacheco, J.F., Sykes, L.R. & Scholz, C.H., 1993. Nature of seismic coupling along simple plate boundaries of the subduction type, *J. geophys. Res.,* **98,** 14 133–14 159.

Rodriguez, M., DeMets, C., Rogers, R., Tenorio, C. & Hernandez, D., 2009. A GPS and modeling study of deformation in northern Central America, *Geophys. J. Int.,* **178,** 1733–1754, doi:10.1111/j.1365-246X.2009.04251.x.

Satake, K., 1994. Mechanics of the 1992 Nicaragua tsunami earthquake, *Geophys. Res. Lett.,* **21,** 2519–2522.

Smith, W.H.F. & Sandwell, D.T., 1997. Global sea floor topography from satellite altimetry and ship depth soundings, *Science,* **277,** 1956–1962.

Stark, P.B. & Parker, R.L., 1995. Bounded-variable least-squares: an algorithm and applications, *Comput. Stat.,* **10,** 129–142.

Turner, H.L.I., LaFemina, P., Saballos, A., Mattioli, G.S., Jansma, P.E. & Dixon, T., 2007. Kinematics of the Nicaraguan forearc from GPS geodesy, *Geophys. Res. Lett.,* **34,** L02302, doi:10.1029/2006GL027586.

Wang, K. & Dixon, T.H., 2004. 'Coupling' semantics and science in earthquake research, *EOS, Trans. Am. geophys. Un.,* **85**(18), 180.

Wessel, P. & Smith, W.H.F., 1991. Free software helps map and display data, *EOS, Trans. Am. geophys. Un.,* **72,** 441–446.

White, R.A., 1991. Tectonic implications of upper-crustal seismicity in Central America in *Neotectonics of North America, Decade Map,* Vol. 1, pp. 323–328, eds Slemmons, D.B., Engdahl, E.R., Zoback, M.D. & Blackwell, D.D., The Geological Society of America, Boulder.

White, R.A. & Harlow, D.H., 1993. Destructive upper-crustal earthquakes of Central America since 1900, *Bull. seism. Soc. Am.,* **83,** 1115–1142.

White, R.A., Ligorria, J.P. & Cifuentes, I.L., 2004. Seismic history of the Middle America subduction zone along El Salvador, Guatemala, and Chiapas, Mexico: 1526-2000, in *Natural Hazards in El Salvador,* Vol. 375, pp. 379–396, eds Rose, W.I., Bommer, J.J.L., Lopez, D., Carr, M.J. & Major, J.J., Geol. Soc. Am. Spec. Pap., The Geological Society of America, Boulder.

Zumberge, J.F., Heflin, M.B., Jefferson, D.C., Watkins, M.M. & Webb, F.H., 1997. Precise point positioning for the efficient and robust analysis of GPS data from large networks, *J. geophys. Res.,* **102,** 5005–5017.